Targeting ferroptosis protects against multiorgan dysfunction and death.

Tom VandenBerghe (tom.vandenberghe@uantwerp.be)
University of Antwerp https://orcid.org/0000-0002-1633-0974

Samya Van Coillie
VIB-Ghent University

Ines Goetschalckx
University of Antwerp

Bartosz Wiernicki
VIB-Ghent University

Banibrata Mukhopadhyay
Muljibhai Patel Society for Research in Nephro-Urology

Wulf Tonnus
University Hospital Carl Gustav Carus at the TechnischeUniversit https://orcid.org/0000-0002-9728-1413

Emily Van San
VIB-Ghent University

Sze Men Choi
University of Ghent

Ria Roelandt
VIB-Ghent University

Catalina Dumitrascu
University of Antwerp

Ludwig Lamberts
University of Antwerp

Wannes Weyts
VIB-Ghent University

Jelle Huysentruyt
VIB-Ghent University

Irina Ingold
Helmholtz Zentrum München

Suhas Lele
Muljibhai Patel Society for Research in Nephro-Urology

Evelyne Meyer
UGent

Ruth Seurinck
VIB-Ghent University https://orcid.org/0000-0002-6636-7572
Yvan Saeys
Ghent University/VIB
An Vermeulen
Ghent University
Alexander van Nuijs
University of Antwerp
Marcus Conrad
Helmholtz Zentrum München https://orcid.org/0000-0003-1140-5612
Andreas Linkermann
Universität Dresden https://orcid.org/0000-0001-6287-9725
Mohan Rajapurkar
Muljibhai Patel Society for Research in Nephro-Urology
Peter Vandenabeele
UGent-VIB https://orcid.org/0000-0002-6669-8822
Eric Hoste
Gent University Hospital
Koen Augustyns
University of Antwerp https://orcid.org/0000-0002-5203-4339

Article

Keywords: ferroptosis, critically ill patients, intensive care unit (ICU)

Posted Date: April 27th, 2021

DOI: https://doi.org/10.21203/rs.3.rs-310675/v1

Version of Record: A version of this preprint was published at Nature Communications on February 24th, 2022. See the published version at https://doi.org/10.1038/s41467-022-28718-6.

Targeting ferroptosis protects against multiorgan dysfunction and death.

Samya Van Coillie[1,2], Ines Goetschalckx[3], Bartosz Wiernicki[1,2], Banibrata Mukhopadhyay[4], Wulf Tonnus[5], Emily Van San[1,2], Sze Men Choi[1,2], Ria Roelandt[1,6], Catalina Dumitrascu[7], Ludwig Lamberts[3], Wannes Weyts[8], Jelle Huysentruyt[1,2], Behrouz Hassannia[1,2], Irina Ingold[9,10], Suhas Lele[4], Evelyne Meyer[11], Ruth Seurinck[1,6], Yvan Saeys[1,6], An Vermeulen[12], Alexander L.N. van Nuijs[7], Marcus Conrad[9,13], Andreas Linkermann[5,14], Mohan Rajapurkar[4], Peter Vandenabeele[1,2,15], Eric Hoste[16], Koen Augustyns[7] and Tom Vanden Berghe[1,2,3*].

[1]VIB-UGent Center for Inflammation Research; Ghent, Belgium.
[2]Department of Biomedical Molecular Biology; Ghent University, Ghent, Belgium.
[3]Department of Biomedical Sciences; University of Antwerp, Antwerp, Belgium.
[4]Department of Nephrology; Muljibhai Patel Society for Research in Nephro-Urology, Nadiad, India.
[5]Department of Internal Medicine 3, University Hospital Carl Gustav Carus; the Technische Universität Dresden, Dresden, Germany.
[6]Department of Applied Mathematics, Computer Science and Statistics; Ghent University Ghent, Belgium.
[7]Department of Pharmaceutical Sciences; University of Antwerp, Antwerp, Belgium.
[8]VIB-UGent Center for Medical Biotechnology; Ghent, Belgium.
[9]Institute of Metabolism and Cell Death, Helmholtz Zentrum München, German Research Center for Environmental Health; Munich, Germany.
[10]Department of Medicine III, Klinikum rechts der Isar; Technical University of Munich, Munich, Germany.
[11]Department of Pharmacology, Toxicology and Biochemistry; Ghent University, Merelbeke, Belgium.
[12]Department of Bioanalysis; Ghent University, Ghent, Belgium.
[13]National Research Medical University, Laboratory of Experimental Oncology; Moscow, Russia.
[14]Biotechnology Center; Technische Universität Dresden, Dresden, Germany.
[15]Methusalem program; Ghent University, Ghent, Belgium.
[16]Department of Internal Medicine; Ghent University Hospital, Ghent, Belgium.

*Correspondence: T.V.B., Universiteitsplein 1, 2610 Antwerp, Belgium, T +3232659250, Tom.VandenBerghe@uantwerp.be, ORCID ID 0000-0002-1633-0974.

Approximately half of all critically ill patients in the intensive care unit (ICU) develop multiorgan dysfunction[1], which is responsible for 30% of deaths worldwide[2,3]. Besides life-supporting treatments, no cure exists for multiorgan dysfunction and its mechanisms are still poorly understood[4]. Catalytic iron is a detrimental factor associated with ICU mortality[5,6] and is known to cause free radical-mediated cellular toxicity[7]. As such, catalytic iron is thought to induce excessive lipid peroxidation[7], the main characteristic of an iron-dependent type of cell death conceptualized as ferroptosis[8,9]. Here we show that pharmacological targeting of ferroptosis with our most potent ferrostatin-analogue[10] rescues from death in acute single and multiorgan dysfunction in mice, but not sepsis. Daily monitoring of critically ill ICU patients revealed that the peak level of malondialdehyde, reflecting excessive lipid peroxidation, correlates with multiorgan dysfunction and death. Our results demonstrate that ferroptosis targeting is life-saving in experimental models of critical illness and that monitoring of malondialdehyde can allow patient stratification. Therefore, controlling the extent of ferroptosis in non-septic patients with multiorgan dysfunction could become a novel treatment for one of the major causes of global deaths.

The authors have declared that no conflict of interest exists.

Patients who suffer from critical illness after an inciting event, for instance major trauma, surgery, or infection[4], frequently require intensive care unit (ICU) support. Critical illness is characterized by multiple organ dysfunction syndrome (MODS), often referred to as multiorgan dysfunction. The extent of organ dysfunction in critically ill patients is correlated to an increase in plasma catalytic iron[6,11,12] also known as labile iron or non-transferrin bound iron, which is a transitional pool of both extra- and intracellular iron. An excess of iron can be sufficient to induce ferroptosis[13,14], a necrotic cell death type caused by iron-dependent peroxidation of polyunsaturated phospholipids in cell membranes[15,16], resulting in cell rupture[17,18]. Therefore, we hypothesized that ferroptosis might be a detrimental factor in multiorgan dysfunction. Noteworthy, iron chelation or treatment with the natural lipophilic radical trap vitamin E, which are both protectants against ferroptosis, have been used to treat iron overdose induced multiorgan dysfunction[19,20].

Plasma catalytic iron and malondialdehyde associate with multiorgan dysfunction and death

To investigate the association between catalytic iron (Fe_c), excessive lipid peroxidation, multiorgan dysfunction and death, the levels of Fe_c and malondialdehyde (MDA), a lipid peroxidation degradation end product, were retrospectively analyzed in plasma of 176 critically ill adult patients enrolled in a prospective cohort study[21]. In this cohort, the median age was 60 (51-70) years. At enrolment, the median sequential organ failure assessment (SOFA) score was 9 (7-11), with 57% of patients suffering from sepsis and 25% of patients having septic shock. The 30-day mortality rate was 23%. To monitor the dynamic fluctuations in these patients, blood was sampled daily for up to 7 days. We found that the maximum value of Fe_c (Fe_c^{max}) per patient showed a significant positive correlation with the SOFA score, reflecting the extent of organ dysfunction (Fig. 1a). The Fe_c^{max} values of patients who succumbed to their illness were significantly higher than those of surviving patients (Fig. 1b), and higher Fe_c^{max} values were found for septic shock patients compared to sepsis patients (Fig. 1c, Extended data Fig. 1a-g). Similarly to Fe_c^{max} values, the maximum value of MDA (MDA^{max}) per patient also showed a significant positive correlation with the SOFA score (Fig. 1d) and was significantly higher in the deceased group than in patients who survived (Fig. 1e). In contrast to Fe_c^{max}, we found no association of MDA^{max} values with either sepsis or septic shock (Fig. 1f and Extended data Fig. 1h-n). It is well-known that an acute phase response during infection upregulates host proteins to control free iron[22], which might explain the dampened ferroptosis signature during sepsis. Consistent with a stronger association of MDA^{max} than Fe_c^{max} with death, only MDA

values were significantly higher in the deceased group when analyzed per day (Extended data Fig. 2a-n). A positive correlation between Fe_c and MDA within patients is evident from the Fe_c levels being significantly higher on the day a patient reached MDA^{max} compared to the day of the minimum MDA value (MDA^{min}) (Fig. 1g). Interestingly, these MDA^{max} values revealed a bimodal distribution for the deceased patients (Fig. 1h). Stratification of all patients based on the local minimum showed that patients with an MDA^{max} >2.85 μM, representing 24.4% of all patients, had a significantly lower survival probability (Fig. 1i). In fact, within this subgroup, 48% deceased within 30-day follow-up. A more stringent selection, based on the local maximum of the second peak (i.e. MDA^{max} of 3.38 μM) resulted in an even higher mortality risk (Extended data Fig. 2o,p). These findings were confirmed by a Cox proportional hazards regression analysis where a 2-fold increase in either MDA^{max} or Fe_c on the corresponding day a patient reached MDA^{max} resulted in an increase of the daily hazard of death of respectively 90 and 40%, after adjustment for age and SOFA score (Extended data Fig. 2q). In summary, these data indicate an association between plasma Fe_c, excessive lipid peroxidation, the development of multiorgan dysfunction, and an increased mortality risk. Patients with septic shock also showed higher maximum levels of Fe_c compared to patients with sepsis, which was not observed for their MDA^{max} values. Hence, ferroptosis targeting should be considered as a therapeutic strategy to dampen excessive lipid peroxidation in non-septic patients with multiorgan dysfunction.

Experimental iron overload induces multiorgan dysfunction through ferroptosis

To mimic increased levels of Fe_c observed in critically ill patients, an experimental iron overload model in C57BL/6N mice was set up. Based on human case reports of iron intoxication, intraperitoneal injection of iron(II) sulphate heptahydrate ($FeSO_4$) was presumed to cause multiorgan dysfunction[19,20]. We determined 300 mg/kg $FeSO_4$ to be the minimal dose needed to overrule the systemic buffer capacity and induce multiorgan injury (Extended data Fig. 3a-d). A steady increase in iron was observed in several organs as a function of time, which was most prominent in the ileum, while plasma iron levels peaked shortly after injection and subsequently dropped (Fig. 2a and Extended data Fig. 3e). Various plasma injury markers were elevated within 30 minutes (min) and all increased further as a function of time (Fig. 2b and Extended data Fig. 3f). Besides measuring plasma lactate hydrogenase (LDH) as a general biomarker for necrosis, we also monitored aspartate aminotransferase (AST) and alanine aminotransferase (ALT) to reflect liver injury, creatinine (Cr) and urea to monitor kidney function, myoglobin (Mb) and creatine kinase (CK) to assess muscle injury, troponin T to

quantify myocardial injury and ferritin to investigate iron dysbiosis. Except for Cr and Mb, which peaked at 2h post-iron overload, all other injury biomarkers peaked at 12h. The exceptionally high levels of CK mainly originated from skeletal muscle tissue, as opposed to heart or smooth muscle tissue (Extended data Fig. 4a-b). MDA levels were determined to monitor excessive lipid peroxidation in multiple organs. A rapid increase, peaking at 30 min to 1h after $FeSO_4$ injection, was observed in kidney, liver, ileum and skeletal muscle tissue, as well as in plasma (Fig. 2c and Extended data Fig. 3g). In addition, an increased number of dead cells as a function of time was detected in kidney, liver and ileum tissue, reflected by a terminal deoxynucleotidyl transferase dUTP nick end labeling (TUNEL) staining (Fig. 2d-g). Hematologic analysis revealed leukocytosis, in particular neutrophilia and lymphopenia, which is also typically observed in patients with acute iron overload[23] (Extended data Fig. 4c,d). Lastly, plasma analysis of a panel of cytokines and chemokines displayed elevated levels of interleukin (IL)-6 upon acute iron overload (Extended data Fig. 4e), likely representing a compensatory mechanism to inhibit intestinal iron uptake through hepcidin upregulation[24].

Increased levels of iron and consequent MDA pointed to the fact that ferroptosis rather than other modes of cell death is primarily responsible for the organ damage. Indeed, mice expressing a kinase dead variant of receptor interacting protein kinase 1 (RIPK1; *Ripk1*$^{ki/ki}$) in which RIPK1 kinase-dependent apoptosis and necroptosis is blocked[25], showed no protection against acute iron overload (Extended data Fig. 5a). Several modes of regulated necrosis mediated by RIPK3, Poly (ADP-Ribose) polymerase 1 (PARP1) and Cyclophilin D (CYPD, encoded by the *ppif* gene) have been reported to contribute to renal ischemia reperfusion injury and/or consequent lung remote injury[26-28]. Upon acute iron overload, mice deficient in RIPK3, CYPD and PARP1 (*Ripk3*$^{-/-}$*;Ppif*$^{-/-}$*;Parp1*$^{-/-}$) only showed a mild drop in some plasma injury biomarkers compared to wild type (WT) mice (Extended data Fig. 5b,d). However, the reduction in organ damage was stronger upon overexpression of glutathione peroxidase 4 (GPX4) (*GPX4*$^{Tg/+}$; Extended data Fig. 5c,e), which inhibits ferroptosis by reducing phospholipid-hydroperoxides to their alcohol form[29]. This protective effect of GPX4 overexpression was also observed in mice triple-deficient in RIPK3, CYPD and PARP1 (Extended data Fig. 5b). As a reverse strategy, we used mice that express a catalytically inactive form of GPX4 (cysteine-variant; *Gpx4*$^{fl/cys}$ R26CreERT2$^{Tg/+}$), referred to as ferroptosis sentinel mice[30]. Due to the inferior reductive capacity of this cysteine-variant to reduce phospholipid-hydroperoxides, these mice are sensitized to ferroptosis[30,31]. When subjected to acute iron overload, they showed a strong sensitization with significantly higher levels of plasma injury biomarkers compared to their littermate controls (Extended data Fig. 6a). Finally, we used a

dietary approach by feeding the mice for 6 weeks with synthetic diets containing different amounts of vitamin E (dl-α-tocopheryl acetate), as a natural lipophilic radical trap inhibiting ferroptosis[32,33]. A high dietary dose of vitamin E reduced the plasma injury biomarkers after iron overload, while a near to deficient vitamin E diet strongly sensitized with sudden death as a result (Extended data Fig. 6b). These findings highlight ferroptosis as a key detrimental factor in iron overload induced multiorgan dysfunction.

UAMC-3203 is a life-saving candidate lead ferroptosis inhibitor protecting against multiorgan dysfunction

The ester-moiety in the ferroptosis inhibitor ferrostatin1 (Fer1) is susceptible to esterase-catalyzed hydrolysis making it unfavorable for *in vivo* use. Therefore, we developed several novel Fer1 analogues with improved stability, efficacy and solubility[10,34]. An *in vivo* pharmacokinetic (PK) study with UAMC-3203 (Fig. 3a), a selected candidate lead inhibitor, was performed in mice after intravenous bolus administration. The plasma concentration-time profile (Extended data Fig. 7a) was best described using a 2-compartment model. A terminal half-life ($t_{1/2}$) of around 3-4h was determined for plasma, kidney, lung, and intestine, with $t_{1/2}$ of muscle being slightly shorter (2h) (Extended data Fig. 7b,c). The median blood to plasma ratio was 0.89 (data not shown), indicating minimal binding to blood cells. UAMC-3203 showed an extensive tissue distribution with tissue-to-plasma ratios ranging from 10.5 to 219. Total exposure (area under the curve, AUC) was about 7 times higher in kidney as compared to intestine and muscle, and about 21 times higher than in lung. Based on the bioanalytical profiles, we predict that UAMC-3203 was metabolized in the liver. In spinal fluid and brain, UAMC-3203 was detected only 15 min after administration, and was not detected at 45 min post-administration, implying no or minor crossing of the blood-brain barrier. Based on the favorable *in vivo* PK profile of UAMC-3203, we first analyzed its efficacy to block iron overload induced multiorgan dysfunction compared to Fer1. UAMC-3203 proved to be superior to Fer1, based on the level of reduction in plasma injury biomarkers LDH, CK, AST and ALT (Fig. 3 b-d and Extended data Fig. 7d), MDA (Fig. 3e), as well as body temperature (Extended data Fig. 7e). Flow cytometric analysis of liver and kidney cell suspensions stained with C11-BODIPY (reflecting lipid peroxidation) illustrated an overall superior *in vivo* dampening of lipid peroxidation by UAMC-3203 compared to Fer1 (Fig. 3f and Extended data Fig. 7f). Interestingly, treatment with UAMC-3203 had no effect on the plasma injury biomarkers in Tumor necrosis factor (TNF)-induced systemic inflammatory response syndrome (Extended data Fig. 8a) or cecal ligation and puncture (CLP) induced septic shock (Extended data Fig. 8b).

Similarly, mice overexpressing GPX4 showed no or even slightly decreased survival after respectively CLP- or lipopolysaccharide (LPS)-induced lethal shock (Extended data Fig. 8c,d). This could imply that ferroptosis inhibition is a promising strategy to control non-septic patients with multiorgan dysfunction (e.g. trauma), while for septic shock patients with multiorgan dysfunction a combination treatment might be needed to control systemic inflammation as well, as we previously reported *viz.* simultaneous neutralization of IL-1 and -18[35]. Noteworthy, reduced levels of plasma iron were detected after TNF or CLP challenge (Extended data Fig. 8e,f), presumably as a protective strategy to limit microbial growth in an attempt to reduce their iron uptake[24,36]. Consequently, the impact of Fe_c-induced multiorgan dysfunction might be less in the case of sepsis or septic shock.

Considering the high mortality in critically ill patients with multiorgan dysfunction, we analyzed the potency of UAMC-3203 to protect against multiorgan dysfunction and death. Using an optimized repeated injection scheme (every 8h), UAMC-3203 almost completely protected against this severe model of iron overload induced lethality (Fig. 3g). To determine the efficacy of UAMC-3203 in blocking ferroptosis in the liver or kidney, we also generated inducible renal tubular epithelial (*Gpx4*^{RTEKO}) and hepatocyte specific *Gpx4*-deficient mice (*Gpx4*^{HEPKO}) (Fig. 3h and Extended data Fig. 9a,b). Both *Gpx4*^{RTEKO} and *Gpx4*^{HEPKO} mice developed respectively ferroptosis-driven acute kidney or liver dysfunction upon tamoxifen (TAM) application and consequently died. Already 6 days after the last TAM injection, *Gpx4*^{RTEKO} mice showed an increase in Cr and urea accompanied by extensive necrosis of the proximal tubules (Fig. 3i,j and Extended data Fig. 9c). In particular, atypical cellular debris in the form of PAS-positive granules was observed, whereas the glomeruli appeared with dilated bowman´s spaces (Fig. 3i). Daily injection of UAMC-3203 following TAM treatment in *Gpx4*^{RTEKO} mice could significantly delay death (Fig. 3k). In renal ischemia reperfusion injury, UAMC-3203 also protected by attenuating tubular damage in the kidney (Extended data Fig. 9d,e). In the case of ferroptosis-driven acute liver injury, *Gpx4*^{HEPKO} mice showed very high ALT, AST and LDH levels concomitant with severe cell death and morphological liver tissue changes (Fig. 3l,m and Extended data Fig. 9f) when sacrificing the mice upon a drop in body temperature. Tissue damage was characterized by enlarged nuclei, chromatin aberrations and paling of both the hepatocellular nuclei and cytoplasm, likely reflecting death cell corpses (Fig. 3l). In the centrilobular region, mild inflammatory infiltrates were detected (Arrow heads Fig. 3l). For *Gpx4*^{HEPKO} mice, UAMC-3203 treatment showed a strong protection against TAM-induced acute liver dysfunction and subsequent death (Fig. 3n), with almost normalized liver plasma injury biomarkers by day 21 when the mice were sacrificed (Extended data Fig. 9g).

This outcome strongly contrasted with the inability of Fer1 to rescue the mice or prolong survival (Fig. 3n). The superior life-saving activity of UAMC-3203 in liver compared to kidney might be due to the conversion of UAMC-3203 in the liver to a more active metabolite, which is still under investigation.

In conclusion, we found that the severity of multiorgan dysfunction and the probability of death among critically ill patients is associated with plasma Fe_c levels and excessive lipid peroxidation. Based on elevated levels of lipid peroxidation, a subpopulation was identified to be at considerably higher risk of death, making MDA measurements a promising prognostic tool. While critical illness displays a high level of complexity, the association of elevated iron and lipid peroxidation levels with poor outcome suggests that ferroptosis can be a detrimental factor during the onset and progression of MODS. These findings shed new light on previous observations in critically ill patients indicating an association between plasma Fe_c[6,11,12] or MDA levels[37,38] and worsening of the disease. Indeed, mirroring increased levels of Fe_c in critically ill patients, we showed that excessive iron is able to induce multiorgan dysfunction in mice, which is dominantly driven by ferroptosis through excessive lipid peroxidation induced injury. This finding strengthens our hypothesis that Fe_c, via oxidation of cellular membrane phospholipids, can initiate ferroptosis and subsequent multiorgan injury in critically ill patients. Here, we show that UAMC-3203 outperforms Fer1 *in vivo* in its ability to reduce multiorgan injury and prevent death. Together, these results uncovered that targeting of ferroptosis might be a valuable novel therapeutic strategy for patients with either acute single or multiorgan dysfunction, which remains one of the major life-threatening conditions in critical illness. Plasma MDA levels can allow patient stratification for future treatment with candidate lead ferroptosis inhibitors. The Fer1-analogue UAMC-3203, or a new derivative thereof, should be considered a superior ferroptosis inhibitor for clinical translation.

AUTHOR CONTRIBUTIONS

Conceptualization, S.V.C., B.H., E.H., K.A. and T.V.B.; Methodology, S.V.C., I.G., B.W., B.M., W.T., E.V.S., S.M.C., C.D., L.L., W.W., J.H. and T.V.B.; Validation, S.V.C., I.G., B.W., and T.V.B.; Formal analysis, S.V.C., R.R., R.S., I.G., B.W., A.V., and A.V.N.; Investigation, S.V.C., I.G., B.W., B.M., W.T., E.V.S., S.M.C., C.D., L.L., W.W., I.I., S.L., and T.V.B. Writing –Original Draft, S.V.C. and T.V.B.; Writing – Review & Editing, S.V.C., B.W., B.H., E.M., M.C., A.L., M.R. and T.V.B.; Funding Acquisition, E.M., Y.S., A.V.N., M.R., P.V., E.H. K.A. and T.V.B.; Resources, E.M. M.C., A.L., K.A., E.H. and T.V.B.; Supervision, E.H. and T.V.B.

ACKNOWLEDGEMENTS

We thank the VIB Flow Core and the VIB Bioimaging Core for training, support, and access to the instrument park and are grateful for the statistical support provided by M. Vuylsteke. We thank C. Peleman for the histopathological descriptions and B. Martin (UAntwerp) for editing the article. The measurement of catalytic iron was performed at the Laboratory of Muljibhai Patel Society for Research in Nephro-Urology, Nadiad, India. This work was supported by the Research Foundation Flanders (FWO) in the form of a predoctoral grant to SVC (1181917N and 1181919N) and the Industrial Research Fund from Ghent University (F2012/IOF-Advanced/001, principal investigators E. Meyer and E. Hoste). B.W. is a PhD fellow paid by UGent Special Research Fund (BOF14/GOA/019), Foundation against Cancer (FAF-F/2016/865), EOS MODEL-IDI (FWO Grant 30837538) and the Odysseus grant 3G0F5716 of Kodi Ravichandran. T.V.B is assistant professor at the University of Antwerp, guest-professor at Ghent University and team leader at the VIB Center for Inflammation Research (IRC). His Ferroptosis and Inflammation Research (FAIR) lab at Ghent University and at the IRC is supported by Excellence of Science EOS MODEL-IDI (FWO Grant 30826052), FWO (G0B7118N), VLIR-UOS (TEAM2018- 01-137, CU2018TEA457A103), Charcot Foundation, Foundation against cancer (FAF-C/2018/1250), Ghent University and VIB. His pathophysiology lab at the university of Antwerp is part of a consortium of excellence focusing on inflammation (INFLA-MED), is supported by Kom op tegen Kanker (G049720N), IOF, TOP-BOF (32254) and FWO (G0C0119N) and has frequent partnerships with international pharma. A.L. is supported by the German Research Foundation (Heisenberg-Professorship 324141047, SFB-TRR 127, SFB-TRR 205, IRTG 2251). M.C. is supported by the Deutsche Forschungsgemeinschaft (DFG) CO 291/7-1, the German Federal Ministry of Education and Research (BMBF) VIP+ program NEUROPROTEKT (03VP04260), the Ministry of Science and Higher Education of the Russian Federation (075-15-2019-1933), and the European Research Council (ERC) under the European Union's Horizon 2020 research and innovation program (grant agreement No. GA 884754). P.V. is senior full professor at Ghent University and senior PI at the VIB Center for Inflammation Research (IRC). Research in his group is supported by EOS MODEL-IDI (FWO Grant 30826052), FWO research grants (G.0E04.16N, G.0C76.18N, G.0B71.18N, G.0B96.20N), Methusalem (BOF09/01M00709 and BOF16/MET_V/007), Foundation against Cancer (F/2016/865, F/2020/1505), CRIG and GIGG consortia, and VIB. E.H is full professor at the Ghent University and staff at the department of Intensive care Medicine, Ghent University Hospital. He is also a senior clinical investigator for the FWO.

DISCLOSURE STATEMENT

T.V.B, P.V. and K. A. hold patents US9862678, WO2016075330, EP3218357 and WO2019154795 related to ferrostatin-1 analogues. M. R. and S. L. report holding United States patents (US 7,927,880 B2 Apr. 19,2011 and US 8,192,997 B2 Jun, 5,2012) and European patents (EP2250500B, 24-04-13) for the methods and kit for the measurement of serum catalytic iron for early detection of acute coronary syndrome and prediction of adverse cardiac events. A.L. issued a patent for Nec-1f, an inhibitor of ferroptosis (20160943.5). M.C. is co-founder and shareholder of ROSCUE Therapeutics GmbH.

REFERENCES

1 Vincent, J. L. *et al.* Comparison of European ICU patients in 2012 (ICON) versus 2002 (SOAP). *Intensive Care Med* **44**, 337-344, doi:10.1007/s00134-017-5043-2 (2018).

2 Fleischmann, C. *et al.* Assessment of Global Incidence and Mortality of Hospital-treated Sepsis. Current Estimates and Limitations. *Am J Respir Crit Care Med* **193**, 259-272, doi:10.1164/rccm.201504-0781OC (2016).

3 Rudd, K. E. *et al.* Global, regional, and national sepsis incidence and mortality, 1990–2017: analysis for the Global Burden of Disease Study. *The Lancet* **395**, 200-211, doi:10.1016/s0140-6736(19)32989-7 PMID - 31954465 (2020).

4 Gourd, N. M. & Nikitas, N. Multiple Organ Dysfunction Syndrome. *J Intensive Care Med* **35**, 1564-1575, doi:10.1177/0885066619871452 (2020).

5 Tacke, F. *et al.* Iron Parameters Determine the Prognosis of Critically Ill Patients. *Crit Care Med* **44**, 1049-1058, doi:10.1097/CCM.0000000000001607 (2016).

6 Leaf, D. E. *et al.* Iron, Hepcidin, and Death in Human AKI. *J Am Soc Nephrol*, doi:10.1681/ASN.2018100979 (2019).

7 Sousa, L., Oliveira, M. M., Pessoa, M. T. C. & Barbosa, L. A. Iron overload: Effects on cellular biochemistry. *Clin Chim Acta* **504**, 180-189, doi:10.1016/j.cca.2019.11.029 (2020).

8 Dixon, S. J. *et al.* Ferroptosis: an iron-dependent form of nonapoptotic cell death. *Cell* **149**, 1060-1072, doi:10.1016/j.cell.2012.03.042 (2012).

9 Friedmann Angeli, J. P. *et al.* Inactivation of the ferroptosis regulator Gpx4 triggers acute renal failure in mice. *Nat Cell Biol* **16**, 1180-1191, doi:10.1038/ncb3064 (2014).

10 Devisscher, L. *et al.* Discovery of Novel, Drug-Like Ferroptosis Inhibitors with in Vivo Efficacy. *J Med Chem* **61**, 10126-10140, doi:10.1021/acs.jmedchem.8b01299 (2018).

11 Leaf, D. E., Rajapurkar, M., Lele, S. S., Mukhopadhyay, B. & Waikar, S. S. Plasma catalytic iron, AKI, and death among critically ill patients. *Clin J Am Soc Nephrol* **9**, 1849-1856, doi:10.2215/CJN.02840314 (2014).

12 Leaf, D. E. *et al.* Increased plasma catalytic iron in patients may mediate acute kidney injury and death following cardiac surgery. *Kidney Int* **87**, 1046-1054, doi:10.1038/ki.2014.374 (2015).

13 Wang, H. *et al.* Characterization of ferroptosis in murine models of hemochromatosis. *Hepatology* **66**, 449-465, doi:10.1002/hep.29117 (2017).
14 Hassannia, B. *et al.* Nano-targeted induction of dual ferroptotic mechanisms eradicates high-risk neuroblastoma. *J Clin Invest* **128**, 3341-3355, doi:10.1172/JCI99032 (2018).
15 Doll, S. *et al.* ACSL4 dictates ferroptosis sensitivity by shaping cellular lipid composition. *Nat Chem Biol* **13**, 91-98, doi:10.1038/nchembio.2239 (2017).
16 Kagan, V. E. *et al.* Oxidized arachidonic and adrenic PEs navigate cells to ferroptosis. *Nat Chem Biol* **13**, 81-90, doi:10.1038/nchembio.2238 (2017).
17 Riegman, M. *et al.* Ferroptosis occurs through an osmotic mechanism and propagates independently of cell rupture. *Nat Cell Biol* **22**, 1042-1048, doi:10.1038/s41556-020-0565-1 (2020).
18 Pedrera, L. *et al.* Ferroptotic pores induce Ca(2+) fluxes and ESCRT-III activation to modulate cell death kinetics. *Cell Death Differ*, doi:10.1038/s41418-020-00691-x (2020).
19 Brown, R. J. & Gray, J. D. The mechanism of acute ferrous sulphate poisoning. *Can Med Assoc J* **73**, 192-197 (1955).
20 Abhilash, K. P., Arul, J. J. & Bala, D. Fatal overdose of iron tablets in adults. *Indian J Crit Care Med* **17**, 311-313, doi:10.4103/0972-5229.120326 (2013).
21 De Loor, J. *et al.* Urinary chitinase 3-like protein 1 for early diagnosis of acute kidney injury: a prospective cohort study in adult critically ill patients. *Crit Care* **20**, 38, doi:10.1186/s13054-016-1192-x (2016).
22 Litton, E. & Lim, J. Iron Metabolism: An Emerging Therapeutic Target in Critical Illness. *Crit Care* **23**, 81, doi:10.1186/s13054-019-2373-1 (2019).
23 Chang, T. P. & Rangan, C. Iron poisoning: a literature-based review of epidemiology, diagnosis, and management. *Pediatr Emerg Care* **27**, 978-985, doi:10.1097/PEC.0b013e3182302604 (2011).
24 Ganz, T. & Nemeth, E. Iron homeostasis in host defence and inflammation. *Nat Rev Immunol* **15**, 500-510, doi:10.1038/nri3863 (2015).
25 Berger, S. B. *et al.* Cutting Edge: RIP1 kinase activity is dispensable for normal development but is a key regulator of inflammation in SHARPIN-deficient mice. *J Immunol* **192**, 5476-5480, doi:10.4049/jimmunol.1400499 (2014).
26 Linkermann, A. *et al.* Two independent pathways of regulated necrosis mediate ischemia-reperfusion injury. *Proc Natl Acad Sci U S A* **110**, 12024-12029, doi:10.1073/pnas.1305538110 (2013).
27 Linkermann, A. *et al.* Synchronized renal tubular cell death involves ferroptosis. *Proc Natl Acad Sci U S A* **111**, 16836-16841, doi:10.1073/pnas.1415518111 (2014).
28 Zhao, H. *et al.* Necroptosis and parthanatos are involved in remote lung injury after receiving ischemic renal allografts in rats. *Kidney Int* **87**, 738-748, doi:10.1038/ki.2014.388 (2015).

29 Seiler, A. *et al.* Glutathione peroxidase 4 senses and translates oxidative stress into 12/15-lipoxygenase dependent- and AIF-mediated cell death. *Cell Metab* **8**, 237-248, doi:10.1016/j.cmet.2008.07.005 (2008).

30 Ingold, I. *et al.* Selenium Utilization by GPX4 Is Required to Prevent Hydroperoxide-Induced Ferroptosis. *Cell* **172**, 409, doi:10.1016/j.cell.2017.11.048 (2018).

31 Ingold, I. *et al.* Selenium Utilization by GPX4 Is Required to Prevent Hydroperoxide-Induced Ferroptosis. *Cell* **172**, 409-422 e421, doi:10.1016/j.cell.2017.11.048 (2018).

32 Carlson, B. A. *et al.* Glutathione peroxidase 4 and vitamin E cooperatively prevent hepatocellular degeneration. *Redox Biol* **9**, 22-31, doi:10.1016/j.redox.2016.05.003 (2016).

33 Wortmann, M. *et al.* Combined deficiency in glutathione peroxidase 4 and vitamin E causes multiorgan thrombus formation and early death in mice. *Circ Res* **113**, 408-417, doi:10.1161/CIRCRESAHA.113.279984 (2013).

34 Hofmans, S. *et al.* Novel Ferroptosis Inhibitors with Improved Potency and ADME Properties. *J Med Chem* **59**, 2041-2053, doi:10.1021/acs.jmedchem.5b01641 (2016).

35 Vanden Berghe, T. *et al.* Simultaneous targeting of IL-1 and IL-18 is required for protection against inflammatory and septic shock. *Am J Respir Crit Care Med* **189**, 282-291, doi:10.1164/rccm.201308-1535OC (2014).

36 Ganz, T. & Nemeth, E. Iron sequestration and anemia of inflammation. *Semin Hematol* **46**, 387-393, doi:10.1053/j.seminhematol.2009.06.001 (2009).

37 Mishra, V., Baines, M., Wenstone, R. & Shenkin, A. Markers of oxidative damage, antioxidant status and clinical outcome in critically ill patients. *Ann Clin Biochem* **42**, 269-276, doi:10.1258/0004563054255461 (2005).

38 Lorente, L. *et al.* Sustained high serum malondialdehyde levels are associated with severity and mortality in septic patients. *Crit Care* **17**, R290, doi:10.1186/cc13155 (2013).

Figures

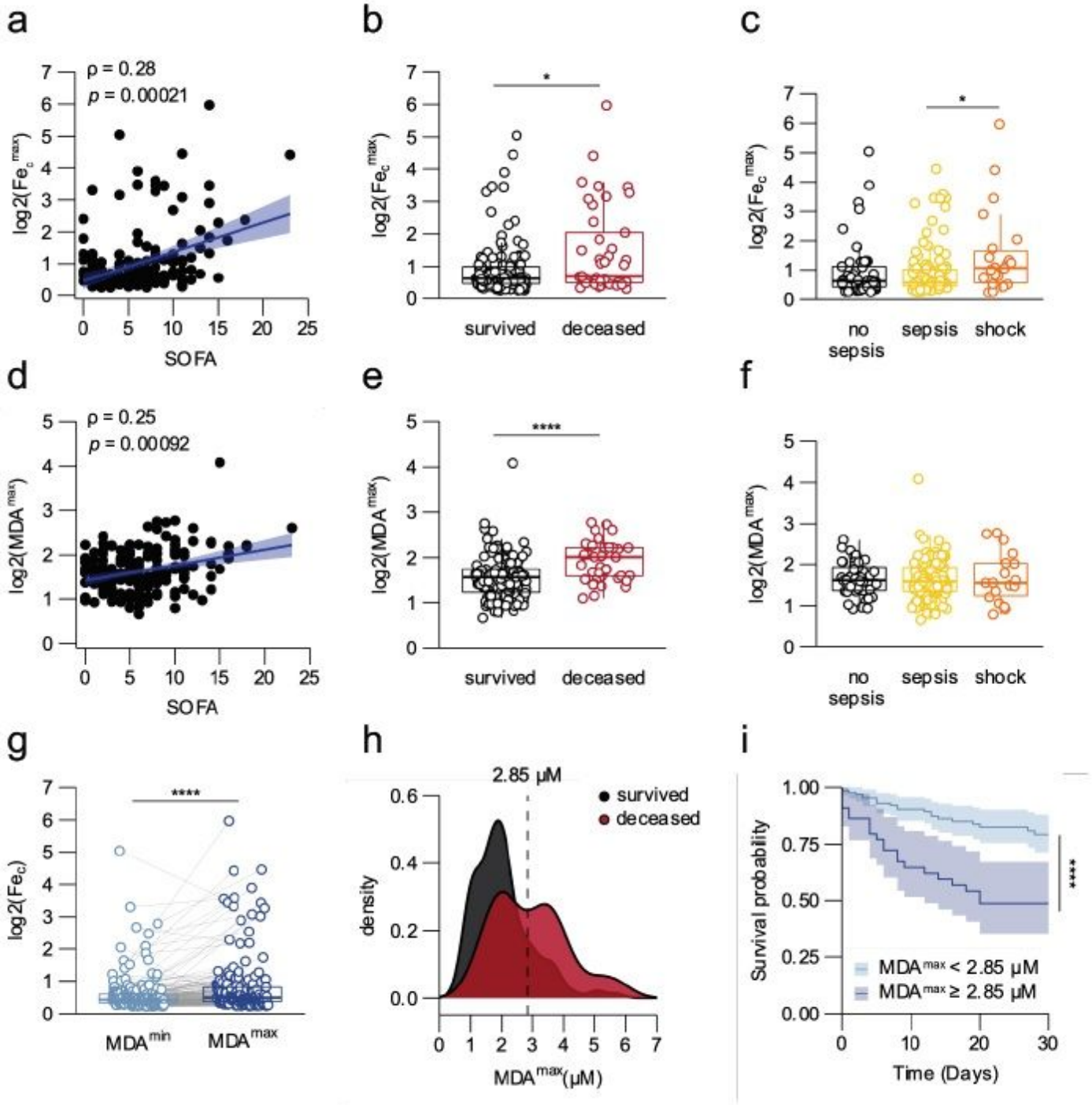

Figure 1

Maximum plasma MDA levels in critically ill patients are associated with plasma catalytic iron (Fec) levels, SOFA score and mortality. a, Scatter plot showing the positive association between the log-transformed values for maximum catalytic iron (Fec max) concentration per patient and the corresponding SOFA scores of that day. b, Boxplots showing the log-transformed Fec max values of

patients who passed away within 30 days and those who survived. c, Boxplots showing the log-transformed Fec max values of all patients grouped by the presence of sepsis, septic shock or non-septic MODS. d, Scatter plot showing the positive association between the log-transformed values for maximum MDA (MDAmax) concentration per patient and the corresponding SOFA scores of that day. e, Boxplots showing the log-transformed MDAmax values of patients who passed away within 30 days and those who survived. f, Boxplots showing the log-transformed MDAmax values of all patients grouped by the presence of sepsis, septic shock or non-septic MODS. g, Boxplots showing the log-transformed Fec values on the day of MDAmin (light blue) and MDAmax (dark blue) for each individual patient (grey lines). h, Histogram representing the density distribution of MDAmax values for both the patients who survived (black) versus those who died (red) within 30 days. i, Survival curves representing the patients with values of MDAmax < 2.85 μM (light blue) and MDAmax ≥ 2.85 μM (dark blue). a, d, Spearman's rank correlation coefficient for continuous variables. b, e, Wilcoxon–Mann–Whitney. c, f, Kruskal-Wallis (omnibus) and Wilcoxon- Mann-Whitney (pairwise) test. g, Paired Wilcoxon signed-rank test. i, Log-Rank test. Error bars represent SEM; *P < 0.05; ****P < 0.0001.

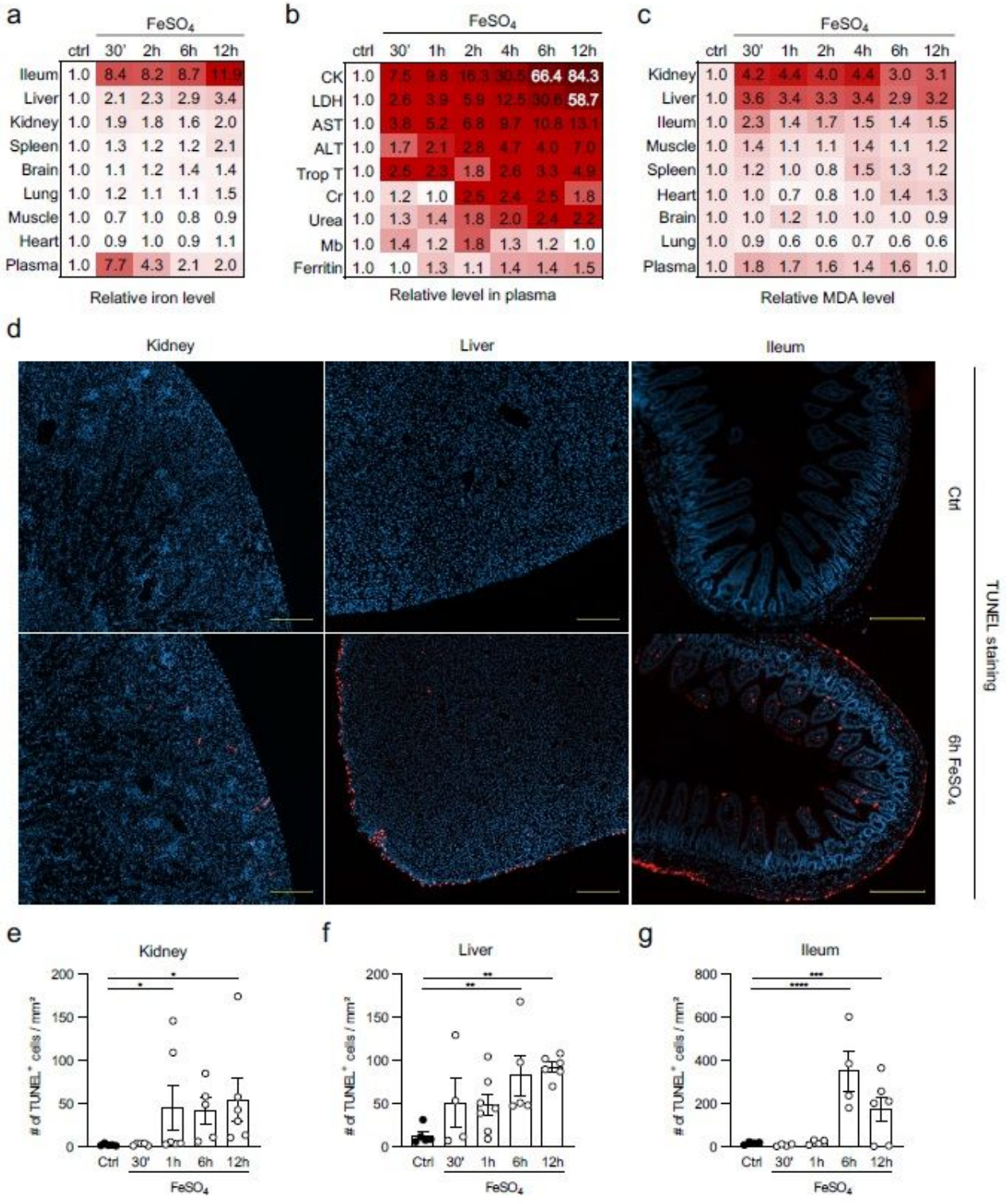

Figure 2

Acute iron overload in mice causes multiorgan failure due to excessive lipid peroxidation. a, Heatmap representing the relative iron levels after acute iron overload as a function of time. The combined results of 3 independent experiments are shown (total n = 5-6/timepoint). b, Heatmap representing the relative increase in creatine kinase (CK), lactate dehydrogenase (LDH), aspartate aminotransferase (AST), alanine aminotransferase (ALT), troponin T (Trop T), creatinine (Cr), urea, myoglobin (Mb) and ferritin after acute

iron overload as a function of time in plasma. The combined results of minimum 3 independent experiments are shown (n = 6-13/time point). c, Heatmap representing the relative MDA levels after acute iron overload as a function of time. The combined results of 3 independent experiments are shown (total n = 5-8/time point). d, Immunohistochemical staining for TUNEL in kidney, liver and ileum 6 h after acute iron overload. Fluorescent photomicrographs representative for the outcome of 3 independent experiments (total n=4-7/ time point) are shown. Scale bar represents 200 μm. e-g, Quantification of immunohistochemical staining for TUNEL in kidney, liver and ileum sections after acute iron overload in function of time. The combined results of 3 independent experiments are shown (total n = 4-7/time point). e, f, g, Pairwise T statistics. Error bars represent SEM; *P < 0.05; **P < 0.01; ***P < 0.001; ****P < 0.0001.

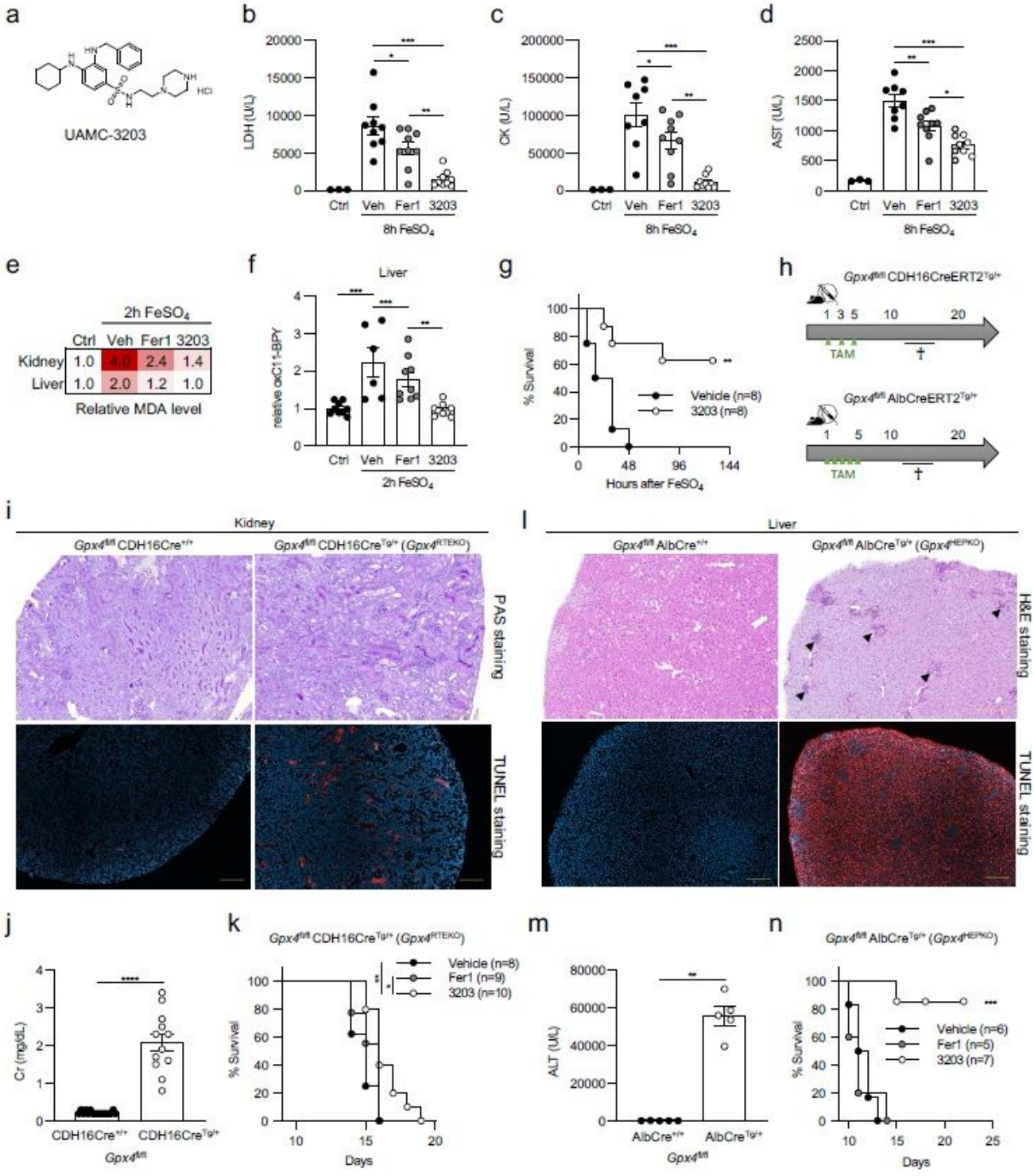

Figure 3

Candidate lead ferroptosis inhibitor (UAMC-3203) is life-saving in different ferroptosis-driven models of (multi)organ injury. a, Chemical structure of UAMC-3203. b-d, Plasma levels of LDH, CK and AST 8h after acute iron overload for mice treated with vehicle (2% DMSO), Fer1, or UAMC-3203. The combined results of minimum 2 independent experiments are shown (total n = 3-9/condition). e, Heatmap representing the relative MDA levels for kidney and liver 2h after acute iron overload for mice treated with vehicle (2%

DMSO), Fer1 or UAMC-3203. The combined results of 2 independent experiments are shown (total n = 5-7/time point). f, Relative measure of lipid peroxidation in liver tissue detected by flow cytometry in the form of oxidized C11- BODIPY (oxC11-BPY) staining 30 min after acute iron overload for mice treated with vehicle (2% DMSO), Fer1 or UAMC-3203. The combined results of 3 independent experiments are shown (total n = 6- 9/condition). g, Survival curve after acute iron overload for mice treated 3 times daily with vehicle (0.9% NaCl) or UAMC-3203. The combined results of 2 independent experiments are shown (total n = 8/group). h, Schematic representation of tamoxifen (TAM) i.p. injection regime (green triangles) of Gpx4fl/fl AlbCreERT2Tg/+ mice or Gpx4fl/fl CDH16CreERT2Tg/+ mice, resulting in respectively acute liver or kidney injury and subsequent death. i, (Immuno)histochemical staining of kidney tissue of Gpx4fl/fl CDH16CreERT2Tg/+ mice which were sacrificed once a human endpoint was reached, with Periodic acid– Schiff's (PAS) and TUNEL staining. Photomicrographs representative for the outcome of 2 independent experiments (total n=6-7/ condition) are shown. Scale bar represents 200 μm. j, Plasma Cr level of Gpx4fl/fl CDH16CreERT2Tg/+ mice which were sacrificed 6 days after TAM administration. The combined results of minimum 2 independent experiments are shown (total n = 10-17/condition). k, Survival curve of Gpx4fl/fl CDH16CreERT2Tg/+ mice treated daily with vehicle (2% DMSO), Fer1 or compound UAMC-3203 starting two days prior to TAM-mediated Cre activation. The combined results of 3 independent experiments are shown (total n = 8-10/group). l, (Immuno)histochemical staining of liver tissue of Gpx4fl/fl AlbCreERT2Tg/+ mice which were sacrificed once a human endpoint was reached, with (on top) H&E and (below) TUNEL staining. Photomicrographs representative for the outcome of 2 independent experiments (total n=8/ condition) are shown. Scale bar represents 200 μm. m, Plasma ALT level of Gpx4fl/fl AlbCreERT2Tg/+ mice which were sacrificed once a human endpoint was reached. The combined results of 2 independent experiments are shown (total n = 5/condition). n, Survival curve of Gpx4fl/fl AlbCreERT2Tg/+ mice treated daily with vehicle (2% DMSO), Fer1 or compound UAMC-3203 starting one day after TAMmediated Cre activation. The combined results of minimum 2 independent experiments are shown (total n = 5-7/group). b, c, d, f, Fisher’s unprotected LSD test. g, m, n, Mantel-Cox test. k, l, Pairwise T statistics. Error bars represent SEM; *P < 0.05; **P < 0.01; ***P < 0.001; ****P < 0.0001.

Supplementary Files

This is a list of supplementary files associated with this preprint. Click to download.

- VanCoillieMXMv7.pdf
- VanCoillieetalExtDataNatureMedv10.pdf